nature communications

Article

https://doi.org/10.1038/s41467-025-66454-9

Shell-isolated nanoparticle-enhanced femtosecond stimulated Raman spectroscopy reveals ultrafast molecular dynamics of surface reactions

Received: 6 April 2025

Accepted: 5 November 2025

Published online: 13 December 2025

Check for updates

Hong-Gang Sun[1,2,10], Yuhan He[3,10], Ling-Yun Hu[2], Renxian Gao[4], Jing-Liang Yang[5], Huijie Liu[2], Xia-Guang Zhang[6], Gui-Lin Yin[2], Bin Hu[2], Zhong-Zhang Shi[2], Ye Yang[2], Yao-Hui Wang[2], Hua Zhang[2,7] ✉, Jinxuan Liu[1,8] ✉, Shisheng Zheng[2], Yu Gu[2] ✉, Zhaohui Wang[2] ✉ & Jian-Feng Li[2,7,8,9] ✉

In-situ tracking of the transient processes of surface/interfacial chemical reactions is of great significance for understanding the essence of catalytic mechanisms but remains highly challenging. Herein, shell-isolated nanoparticle-enhanced femtosecond stimulated Raman spectroscopy (SHINE-FSRS) with high sensitivity and temporal resolution has been developed to explore the ultrafast molecular dynamics of surface reactions. The FSRS signals have been greatly enhanced through the fabrication of plasmonic nanocavities, achieving a maximum enhancement factor of ~10^6 through optimal matching of the plasmonic band of the nanocavity with the wavelength of the Raman pump laser, using malachite green (MG) as the probe molecule. Using SHINE-FSRS, the ultrafast structural evolution during the photo-induced reaction of malachite green molecules adsorbed on Au or Ag surfaces has been successfully in-situ monitored at the femtosecond timescale. Direct spectroscopic evidence reveals that malachite green undergoes intramolecular twisting with 100 fs, and the strong localized plasmonic field can accelerate the twisting process. This work showcases the capability of SHINE-FSRS to effectively probe the molecular structural evolution of surface species during reactions with high temporal resolution, underscoring its potential for in-situ investigations of surface and interfacial catalytic processes.

In-situ monitoring of the dynamic processes of chemical reactions and identifying the molecular structure of key reaction intermediates are of great significance for elucidating molecular reaction mechanisms[1–4]. Normal Raman spectroscopy[5] or infrared spectroscopy (IR)[6] is a versatile tool to reveal the fingerprint structures of steady species, but is often frustrated for the dynamic study, especially in detecting the key intermediates within extremely short lifetimes (from femtoseconds to nanoseconds). The transient absorption (TA) spectroscopy[7,8] can capture the electronic relative process with temporal resolution up to femtoseconds, but it still remains a significant challenge to reveal the molecular structures of short-lived intermediates.

A full list of affiliations appears at the end of the paper. ✉e-mail: zhanghua@xmu.edu.cn; jinxuan.liu@dlut.edu.cn; ygu@xmu.edu.cn; zhwang@xmu.edu.cn; li@xmu.edu.cn

With the development of femtosecond laser technology, femtosecond stimulated Raman spectroscopy (FSRS)[9,10] has emerged as a powerful vibrational spectroscopy. In FSRS, the temporal overlap between Raman pump and probe pulses (typically, a femtosecond white light continuum (WLC)) creates the population at the vibrational excited state and slices the target dynamics with femtosecond temporal resolution firstly. Then the picosecond Raman pump reads out the vibration population at the following process and provides a high-frequency resolution[11,12]. Thus, high temporal and frequency resolution can be achieved simultaneously with the measurement at different delays[13,14]. FSRS can reveal molecular structures and properties, such as the magnitude of the bond strengths, the nature of chemical environments, and even the characteristics of the electronically excited state[9,15,16]. By employing the pump-probe technique, FSRS represents a fundamental advancement in the quest for real-time structural measurements of chemical transformations[17–19].

To further improve the sensitivity and generality of Raman spectroscopy, our group invented a technique named shell-isolated nanoparticle-enhanced Raman spectroscopy (SHINERS)[20,21]. The underlying principle of SHINERS involves chemically coating an ultra-thin (~2 nm) silica shell onto gold nanoparticles (Au NPs), creating shell-isolated nanoparticles (SHINs)[22–24]. The Au core can generate strong localized electromagnetic fields to amplify the Raman signals of molecules near SHINs, while the silica shell serves as a chemical protector that isolates the Au core from the external environment. This design preserves the enhancement effect while avoiding the charge exchange between Au and its surroundings[25]. Such a shell-isolated enhanced mode has also been successfully expanded to other techniques to improve their sensitivity[26], such as tip-enhanced Raman spectroscopy, sum frequency generation, second harmonic generation, fluorescence, and even mass spectrometry[27–30].

Herein, we developed shell-isolated nanoparticle-enhanced femtosecond stimulated Raman spectroscopy (SHINE-FSRS) with ultrahigh sensitivity and temporal resolution by combining SHINERS and FSRS, and achieved the in-situ monitoring of the ultrafast molecular dynamics of surface reactions (Fig. 1a, b). Meanwhile, Raman-induced Kerr effect (RIKE) spectroscopy has been adopted to address the limitations of traditional FSRS, such as dispersive line shapes[31,32] and intense probe background. The correlation between the Raman enhancement and excitation wavelengths has been explored in a home-built FSRS setup (Fig. 1c), and a maximum Raman enhancement factor of ~10^6 has been obtained for various probe molecules when the excitation wavelength matches with the plasmonic band of SHINs. Using the SHINE-FSRS, we monitored ultrafast dynamics of photo-induced process of MG molecule adsorbed on Au surfaces. It is found that the MG molecule would undergo intramolecular twisting within 100 fs, and the strong localized plasmonic field can accelerate the structural evolution process.

Results and Discussion

Development of SHINE-FSRS methodology

Here, we propose a SHINE-FSRS method by combining SHINERS with FSRS (Fig. 1a–c). RIKE has been introduced by employing a circularly polarized Raman pump via a quarter-wave plate and crossed polarizers in the probe path (Fig. 1c)[33–36]. A polarizer, half-wave plate, and quarter-wave plate (fixed at 45°) in the Raman pump path generate circularly polarized light, enabling crossed polarizers to suppress ~99% of the probe background while preserving the Raman signal via the Kerr effect. This configuration not only eliminates the white light interference, allowing extended integration for detecting the weak interfacial signals, but also circumvents the dispersive line profiles inherent in conventional FSRS[37], thereby facilitating the acquisition of symmetric vibrational spectra with an enhanced signal-to-noise ratio (Supplementary Fig. 1). Meanwhile, we implemented a chopper–Galvo synchronized system that spatially and temporally isolates pump-on/off signals through 1 kHz modulation coupled with probe beam

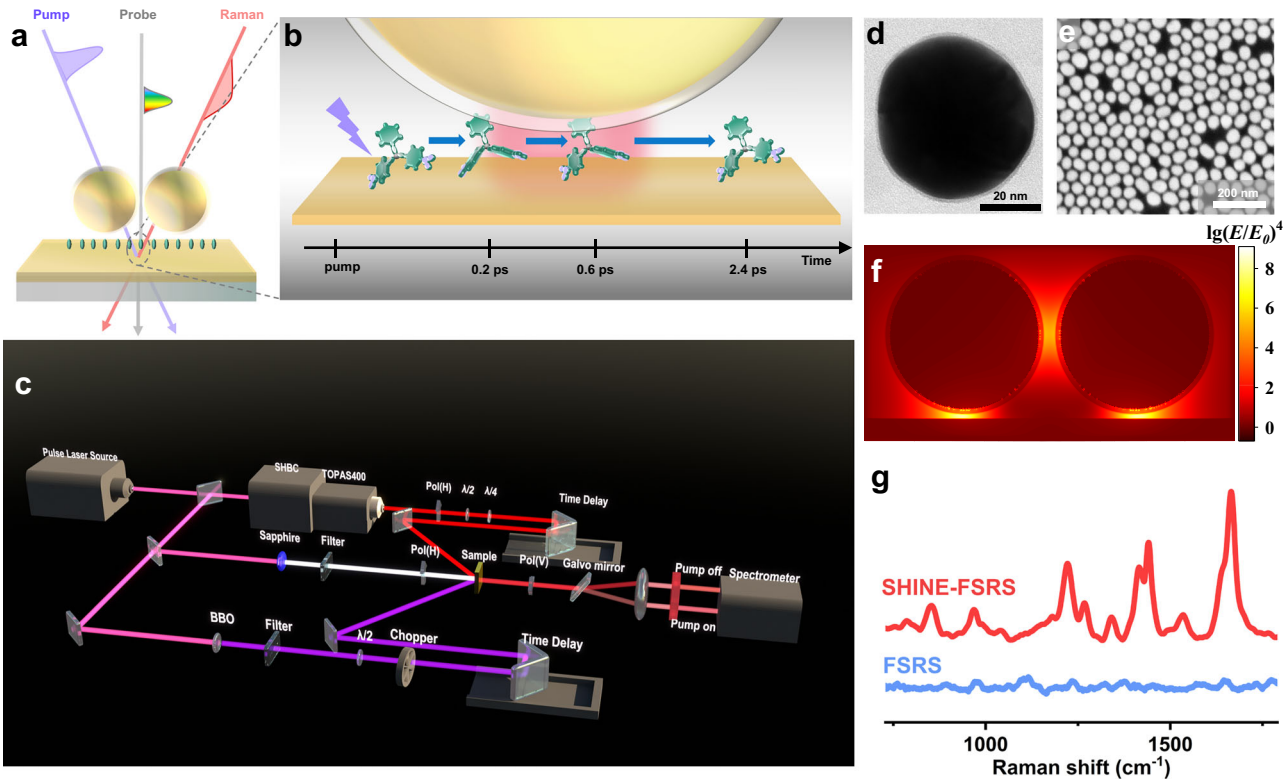

Fig. 1 | Filming molecular movie through SHINE-FSRS. a Concept image of this work. **b** Schematic diagram of the molecular movie. **c** Schematic diagram of FSRS experimental set up. **d**, **e** TEM and SEM images of Au SHINs. **f** A 3D-FDTD simulation for a SHINs dimer on Au film under 640 nm electromagnetic plane wave, where E and E_0 denote the localized electric field and the incident electric field. **g** FSRS spectra of MG with and without SHINs.

dithering. Time-resolved Raman spectra were acquired using a normalized differential approach; by subtracting the Raman spectrum without the 400 nm pump pulse from that with the pump pulse at specific time delays (Fig. 1c).

We deposited ~20 nm Au film on a quartz wafer as the substrate of sample, so that it can transmit light while generating surface plasmon resonance (SPR). SHINs with a shell thickness of ~2 nm were self-assembled to form a mono-layer on the Au film adsorbed with probe molecules (Fig. 1d, e). Under light irradiation with a specific wavelength, the Au SHINs can generate a strongly coupling effect with SPR generated on the Au film, significantly enhancing the electromagnetic field intensity within a narrow range in the nanocavity between the SHINs and the substrate[38]. The localized surface plasmon resonance (LSPR) of the sample can be derived from the dark-field scattering shown in Supplementary Fig. 2. A broad scattering peak ranges from 550 nm to 800 nm indicating SERS ability of the sample. This localized electric field enhancement effect has been proven to be widely applicable in various spectroscopic techniques, such as Raman spectroscopy, fluorescence, second harmonic generation, and sum frequency generation[39–41].

Three-dimensional finite differential time-domain (3D-FDTD) simulation was conducted to calculate the electric field distribution surrounding SHINs and Au film under 640 nm circularly polarize electromagnetic wave excitation. Strong electromagnetic fields are observed in the nanocavity between Au SHINs and the Au substrate, and the Raman signals of the molecules located at these hot spots can be enhanced by more than seven orders of magnitude (Fig. 1f). The stimulated Raman spectra were conducted on an Au film adsorbed with MG molecules in the presence and absence of SHINs (Fig. 1g). It can be seen that SHINE-FSRS significantly amplifies the SRS signal, while no signals of MG are observed for normal SRS.

The SHINE-FSRS with different polarized Raman pump is present at Supplementary Fig. 3. The left circle polarized Raman pump can keep the enough Raman signal while the baseline aroused from the non-resonant signal is very small. Although the linear polarized Raman pump leads to larger Raman signal, the non-linear signal would also be larger. Thus, the Raman pump was set to left circle Raman pump. Meanwhile, the spectral intensity is proportional to the square of pump intensity (Supplementary Fig. 4). At the following experiments, the Raman pump power was optimized to ~200 nJ. Higher power would easily lead to sample damage and the lower power need a long time to obtained a quality spectrum.

The enhancement factor of SHINE-FSRS was quantitatively investigated using 4-nitrobenzenethiol (pNTP), phenyl isocyanide (PIC), and MG as probe molecules. The Raman intensity of each molecule varies with Raman pump wavelength (Fig. 2a–c). The trend of variation is consistent with the dark field scattering spectrum of SHINs (Fig. 2d, Supplementary Fig. 2), indicating the Raman enhancement originates from the plasmonic effect of SHINs. The maximum enhancement factor of SHINE-FSRS, obtained at 640 nm, when their corresponding wavelength falls around 710 nm, the SPR resonant wavelength. The result indicated that the enhancement is associated with radiational enhancement[42,43]. The enhancement factor (EF) is up to ~10^6, and the EFs of different molecules are on the same order of magnitude (Fig. 2e), indicating that EF is primarily driven by the electric field generated by the SHINs, with minimal interference from the electronic resonance (Supplementary Fig. 5)[44].

Transient reflection spectroscopy revealing electronic dynamics of MG

In order to investigate the relaxation of the excited states of MG molecules, we used transient reflection spectroscopy to test MG adsorbed on an Au substrate (Supplementary Fig. 6). We select a 400 nm femtosecond pulse laser as the actinic pump, and a supercontinuum white light as the probe. The MG molecules are placed in the gap between SHINs and Au substrate (see detailed experimental procedure in the "Methods" section). The transient reflection spectral map of the sample contains three sets of transient characteristics, corresponding to molecules at different electronic energy states (Fig. 3a). We extracted three kinetic characteristic curves from the spectrum with a singular value decomposition algorithm (Fig. 3b), the broad absorption band at 550–720 nm can be attributed to ground state bleaching (GSB) of MG molecules according to the steady absorption spectroscopy (Supplementary Fig. 7). The fitting result indicates a rising time of about 0.3 ps and a relaxing time of about 1.95 ps. The transient signal at 760-880 nm corresponds to the $S_1 \rightarrow S_0$ emission according to the steady emission spectroscopy (fluorescence spectroscopy, Supplementary Fig. 8). The kinetics at 760-880 nm can be fitted by a two-exponential function with time constants of 0.3 ps and 0.6 ps. The first-time constant originates from an internal conversion process from $S_2 \rightarrow S_1$, while the second time constant originates from an internal conversion from S_1 to S_0 (Supplementary Fig. 9). As the S_2 excited state emission band decays, the S_1 excited state emission band gradually grows and decays with a time constant of 2 ps. Thus, we can reconstruct the process of MG molecules transferring between different electronic states after being excited by a 400 nm pulse. Under femtosecond pulse excitation at 3.1 eV, corresponding to the $S_0 \rightarrow S_2$ energy gap (Supplementary table 2), the molecule is excited from S_0 to the S_2 state and relaxed to the S_1 state, and then returns to the ground state (Fig. 3e).

SHINE-FSRS revealing structural changes of MG

To elucidate the evolution of the molecular structure of MG molecules during excited state relaxation, time-resolved in-situ SHINE-FSRS has been employed to monitor the reaction. We employed the narrow Raman pump at 640 nm and the broadband (400–800 nm) supercontinuum white light to obtain stimulated Raman signals. The femtosecond stimulated Raman spectra of the samples under a 400 nm actinic pump (Fig. 3c) were presented as the difference between the spectra with and without the actinic pump pulse. The main bands were the in-plane ring deformation + C–H in-plane bending ($\alpha_{ring} + \beta_H$) at 1250 cm^{-1}, and the N–ph–C skeleton asymmetric and symmetric stretching at 1400 cm^{-1} and 1440 cm^{-1}, respectively. Detailed Raman band assignments are given based on DFT calculation and listed (Supplementary table 1).

The kinetics of the photo-induced MG reaction can be obtained based on the evolution of the intensities of the characteristic Raman bands. Figure 3d displays the normalized intensity of the three Raman peaks (1250 cm^{-1}, 1400 cm^{-1}, and 1440 cm^{-1}) as a function of the delay time between the 400 nm actinic pump pulse and the SHINE-FSRS signal acquisition. It can be seen that the kinetic curves of these three Raman peaks show an exponential decay with different lifetimes and are in one-to-one correspondence with transient reflection results (Supplementary table 3). The relaxation time of the Raman band at 1400 cm^{-1} (2.0 ps) matches the time scale of GSB in transient reflection spectra (2.4 ps), indicating that the molecular skeleton of MG molecules undergoes deformation after excitation. The Raman band at 1440 cm^{-1} shares the same time constant with S_2 excited state emission. Thus, it can be assigned to N–ph–C skeleton symmetric stretching mode of MG at S_2 excited state. The Raman band at 1250 cm^{-1} can be assigned to $\alpha_{ring} + \beta_H$ of MG at S_1 state. Thereby, we successfully observed the evolution of the molecular structure of excited MG molecules using SHINE-FSRS. The distinct kinetics of different vibrational modes, along with their one-to-one correspondence with the dynamics observed in transient reflection spectra, indicate that electronic excitation initiates subsequent geometric restructuring. According to these findings, we therefore hypothesize that the observed dynamics originate from intramolecular twisting triggered by the altered electronic distribution in the excited state.

To verify this hypothesis, we performed density function theory (DFT) to calculate the Raman cross-section of molecules at different

https://doi.org/10.1038/s41467-025-66454-9

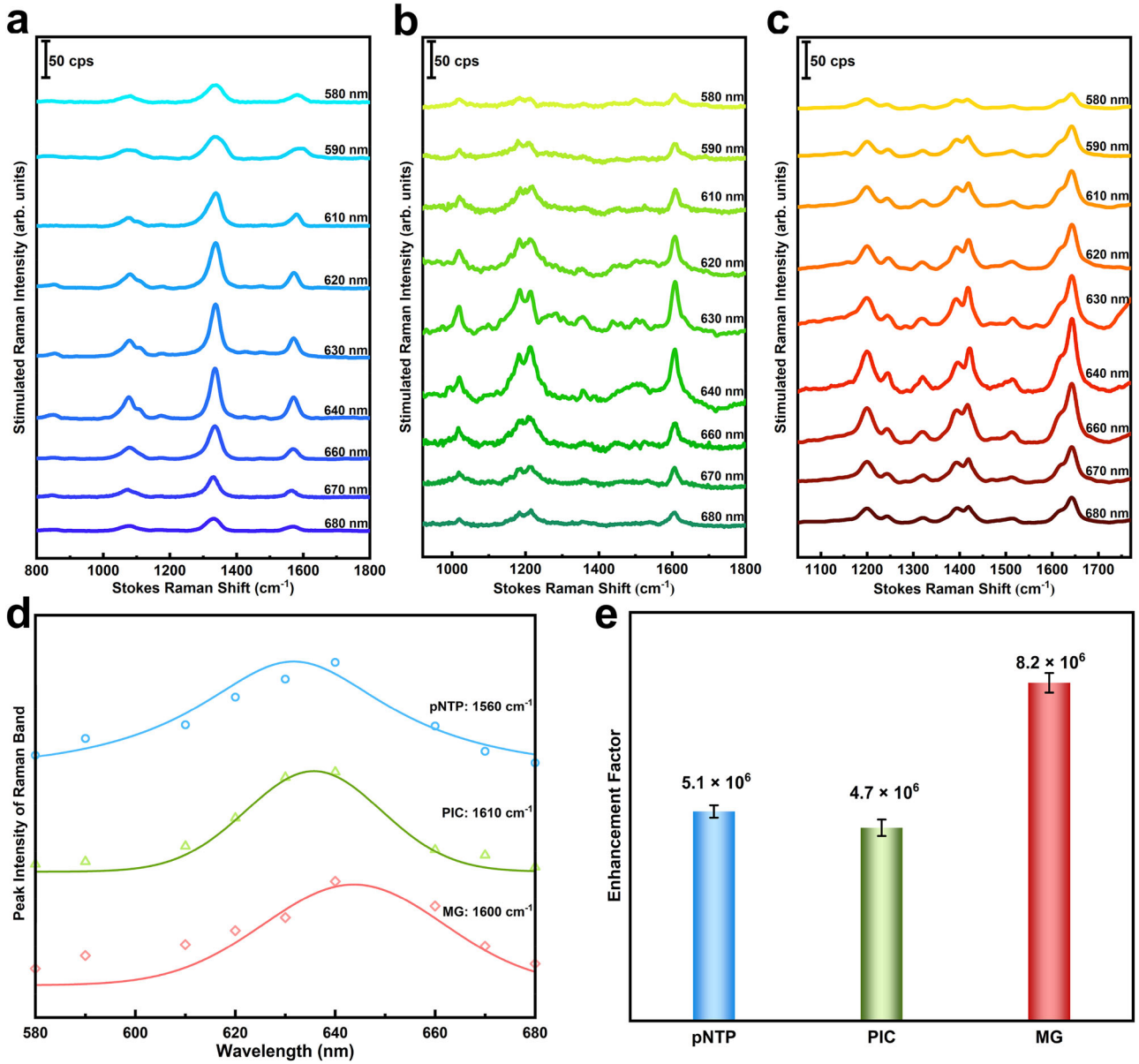

Fig. 2 | The enhancement factor of SHINE-FSRS. a–**c** SHINE-FSRS spectra of pNTP, PIC, and MG with different Raman pump wavelengths, respectively. cps, counts per second. **d** The variation of the main Raman peak intensity of different molecules as a function of the Raman pump wavelength. The symbols and solid lines represent the experimentally measured data and the trend curve, respectively. **e** Calculated enhancement factors for different probe molecules. The error bars represent standard error of the mean ($n = 3$ independent experiments), the values displayed above the bars represent the average calculated enhancement factor for each molecule.

torsion angles. The configurations of MG at different electronic states with minimum energy are calculated and shown in Fig. 3e. We calculated the Raman spectra of the molecule in the saddle point configuration of the potential energy surface, and extracted three vibrational modes with Raman shifts of 1255 cm^{-1}, 1400 cm^{-1}, and 1440 cm^{-1} from the results. It can be seen that the Raman cross-section of vibrational modes with Raman shifts of 1255 cm^{-1} and 1400 cm^{-1} increase with increasing torsion angle, while the 1440 cm^{-1} mode decrease. These results verify our hypothesis that intramolecular torsion occurs in MG after excitation (Supplementary Fig. 10b)[45].

Plasma-induced resonance energy transfer produced by Ag SHINs

Plasmon-induced resonance energy transfer between plasmonic materials and molecules has been proven to be a promising pathway to accelerate excited state relaxing[38,46]. The results in Fig. 3 was obtained using Au SHINs as the Raman amplifiers. As the LSPR band of Au nanoparticles is located at > 500 nm, the 400 nm pump cannot excite the LSPR effect of Au. Compared with Au, the plasmonic band of Ag nanoparticles is located at a shorter wavelength range. Therefore, Ag SHINs may generate stronger plasmonic electromagnetic fields under the 400 nm pump, thus accelerating the photo-induced reaction of MG.

To reveal the role of plasmonic effect in the photo-induced reaction of MG, we further investigated the ultrafast reaction dynamics by putting MG molecules in the nanocavity between Ag SHINs and Ag substrate using SHINE-FSRS (Fig. 4a). We observed similar Raman features as those obtained when using Au SHINs. However, compared with Au SHINs, the excited state signal lifetime of MG molecules is much shorter for Ag SHINs. We extracted the kinetic curves of the Raman peak located at 1400 cm^{-1} of two types of SHINs, and plotted them in the same diagram.

https://doi.org/10.1038/s41467-025-66454-9

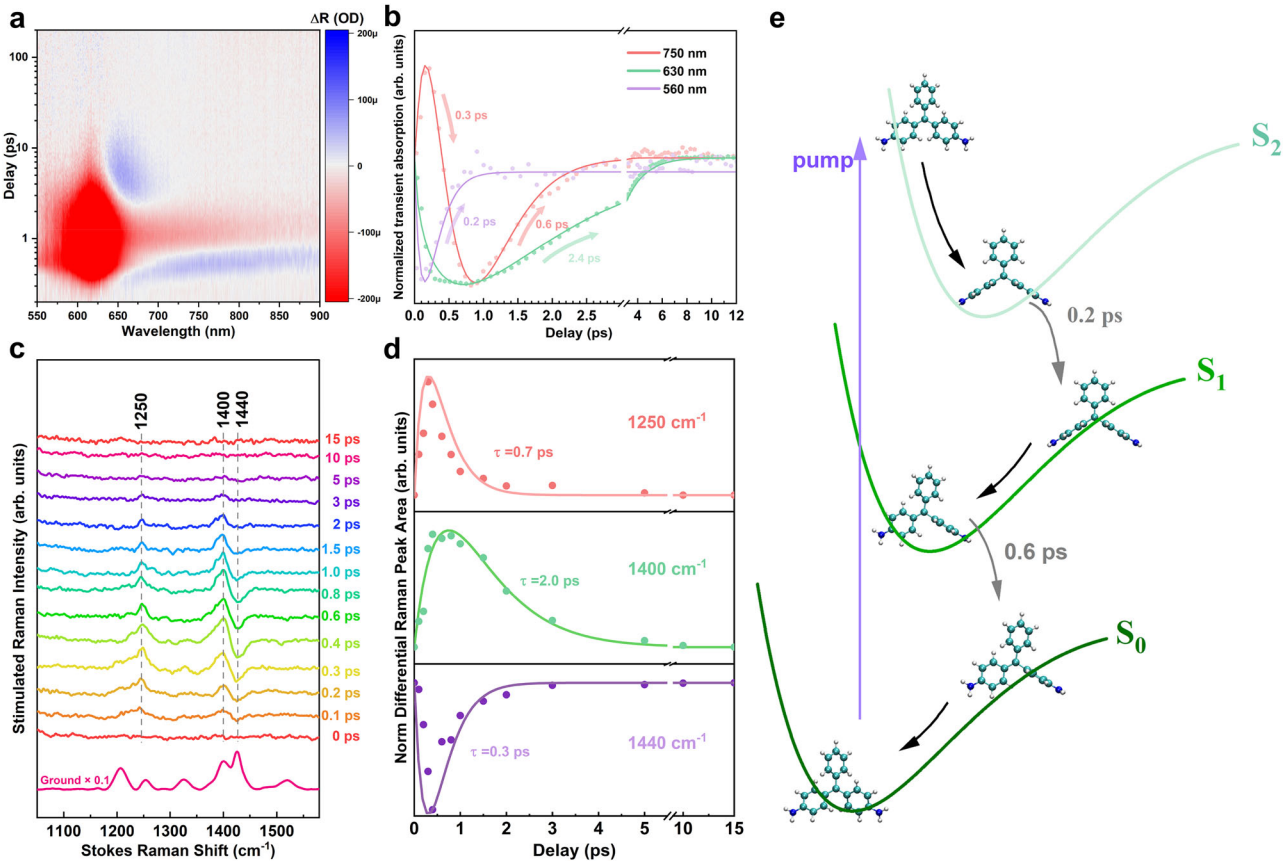

Fig. 3 | Ultrafast dynamic of MG. a Transient reflection spectral map of the sample. **b** Kinetics at 750 nm, 630 nm, and 560 nm. The dots and solid lines represent the experimentally measured kinetic data and the fitted kinetic curve, respectively. **c** SHINE-FSRS spectra of the sample, obtained with 640 nm Raman pump and 400 nm actinic pump. The spectrum represents the normalized difference between the data collected with and without the actinic pulse. The dashed lines highlight the peak positions that exhibit notable spectral changes. **d** Kinetics at 1250 cm^{-1}, 1400 cm^{-1}, and 1440 cm^{-1}. The dots: the experimentally measured data. The solid lines: the fitted data. **e** Schematic illustration of the potential energy surfaces of MG at different states and the lowest energy configuration of each state.

Detailed kinetic fittings of MG within Ag SHINs are shown in Fig. 4b. In the presence of Ag SHINs, the excited state signal of MG molecules undergoes a ~1 ps relaxation, which is much faster than that for Au SHINs (~5 ps) (Fig. 4b). Meanwhile, unlike Au SHINs, three characteristic Raman features decay with almost the same time constant. This indicates that Ag SHINs alter the excited state relaxation pathways of MG. We compared the transient reflection spectra of the MG on quartz and Au/Ag SHINs (see Supplementary Fig. 11). The kinetic features of MG on quartz and within Au SHINs show no apparent difference, indicating that Au SHINs does not significantly affect the molecular excited state dynamics. However, we did not observe any MG transient signal within Ag SHINs. This is probably because the opto-induced strong coherent acoustic vibrations conceal any transient signal generated by MG. Therefore, we can only investigate this phenomenon from the perspective of the influence of the localized plasmonic field on the emission of molecular excited states.

Previous works have reported that photonic environment can modify the emission rate of the emitters, known as the Purcell effect[47,48]. The Purcell effect consists two parts: enhanced excitation and enhanced emission rate. We performed 3D-FDTD to simulate the electromagnetic field distribution under 400 nm excitation (Fig. 4c) and emission rate enhancement of MG molecules within Au and Ag SHINs (Fig. 4d)[49,50]. In brief, the emission rate of MG γ_{emi} in the presence of Au/Ag SHINs by the excitation rate γ_{exc} and the quantum efficiency (QE):

$$\gamma_{emi} = \gamma_{exc} \cdot QE \quad (1)$$

where, γ_{exc} can be estimated as the square of the plasmonic field. The plasmonic field generated at the gap between Ag SHINs and Ag substrate is much stronger than that between Au SHINs and Au substrate (Fig. 4c). The averaged E/E_0 values in the nano-gap from Fig. 4c were taken to estimate γ_{exc}, which is 1.4 for Au SHINs and 10.2 for Ag SHINs. The QE is the ratio between the decay rate due to radiative transitions and the total decay rate, which is a function of the emission wavelength. The results are plotted in Fig. 4d. For Au SHINs, the emission rate enhancement is close to 1, as MG's $S_2 \rightarrow S_0$ emission processes do not overlap with Au SHINs' SPR band (Supplementary Fig. 2). The kinetics of MG in ethanol show no obvious difference compared to MG with Au SHINs further confirmed the weak interactions between the MG molecules and Au SHINs (Supplementary Fig. 12)[51]. For Ag SHINs, the emission rate enhancements for $S_2 \rightarrow S_0$ and $S_1 \rightarrow S_0$ are ~8-fold and 10-fold, respectively, due to their SPR band aligning with MG's emission bands (Supplementary Fig. 2). These findings are consistent with ultrafast Raman results. The fluorescence intensity of Ag SHINs is ~10 times greater than that of Au SHINs at around 750 nm and ~5 times greater at around 560 nm, as evidenced by the enhanced fluorescence spectra (Supplementary Fig. 8) further confirm Ag SHINs' enhancement of MG's emission. These results proved the acceleration of the molecular dynamic caused by localized plasmonic field, providing direct experimental evidence for understanding fundamental mechanism of plasmon-molecules interactions and plasmon-enhanced photocatalysis.

In summary, we have established a SHINE-FSRS method that has ultrahigh sensitivity and temporal resolution. By putting molecules in the nanocavity between Au/Ag SHINs and Au/Ag substrates, the FSRS

https://doi.org/10.1038/s41467-025-66454-9

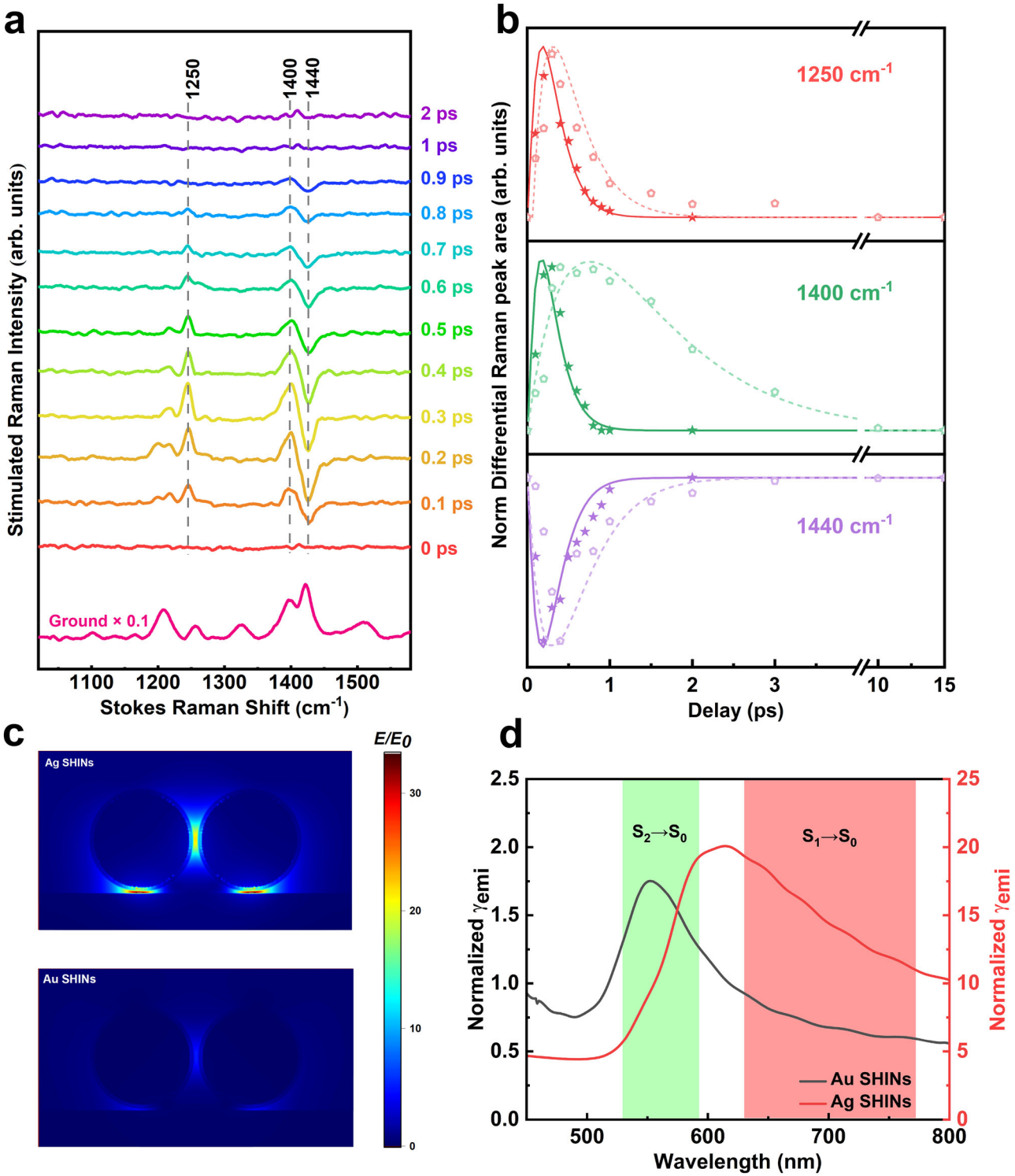

Fig. 4 | Comparison of Au & Ag SHINs. a SHINE-FSRS spectra of the sample with Ag SHINs, obtained with 640 nm Raman pump and 400 nm actinic pump. The spectra represent the normalized difference between the data collected with and without the actinic pulse. The dashed lines highlight the peak positions that exhibit notable spectral changes. **b** Comparison of kinetics of the sample with Au & Ag SHINs at 1250 cm^{-1}, 1400 cm^{-1}, and 1440 cm^{-1}. The circles and pentagrams represent the experimentally measured kinetic data for the Au SHINs and Ag SHINs systems, respectively, while the dashed and solid lines correspond to the fitted kinetic data for the Au SHINs and Ag SHINs systems, respectively. **c** Simulated electric field intensity distribution of Ag (up) and Au (down) SHINs dimer on Au/Ag substrates under 400 nm plane electromagnetic wave. **d** The acceleration rate of MG molecules with Au and Ag SHINs. Black: Au SHINs; Red: Ag SHINs. Green and red shades mark the peak locations of $S_2 \rightarrow S_0$ and $S_1 \rightarrow S_0$.

signals of surface species can be enhanced, thus allowing the in-situ monitoring of ultrafast surface reaction processes on the picosecond or even femtosecond timescale. The enhancement is strongly dependent on the matching degree between the Raman pump and the plasmonic band of SHINs, and a maximum enhancement factor of ~10^6 has been obtained. Using SHINE-FSRS, the ultrafast molecular dynamic process of the photo-induced reaction of MG molecules adsorbed on Au surfaces has been in-situ studied. Direct spectroscopic evidence,

combining DFT simulations, demonstrates that MG would undergo intramolecular torsion with 1 ps under the excitation of a 400 nm pulse laser. Meanwhile, it is found that Ag SHINs can generate strong plasmonic fields under such excitation conditions. This can greatly accelerate the photo-induced reaction of MG, leading to the relaxation time decrease from ~5 ps to ~1 ps. The SHINE-FSRS method developed in this work can effectively study the structural evolution of surface species during reactions with ultrahigh temporal resolution, thus exhibiting great potential in the in-situ study of surface/interface catalytic processes.

Methods

Preparation of Au and Ag SHINs

Gold nanospheres were prepared according to the method of Frens. First, 1.4 mL of sodium citrate solution (1 wt.%) was added to 200 mL of boiling chloroauric acid solution (0.01 wt.%). The mixture was refluxed for 1 h and then cooled to room temperature to obtain 55-nm bare Au nanoparticles. A silica shell was coated on the bare Au nanoparticles[35]. First, 0.4 mL of (3-aminopropyl) trimethoxysilane solution (1 mM) was mixed with 30 mL of previously prepared bare Au nanoparticle solution. Next, 3 mL of sodium silicate solution (0.54 wt.%) was added, and the resulting mixture was placed in a water bath at 95 °C for 15 min. This resulted in the coating of a 2 nm silica shell. The Au@SiO_2 SHINs were centrifuged at 5500 × *g* and washed twice with Milli-Q water.

Silver nanospheres were prepared as the following procedures. First, 10 mL of sodium citrate solution (1 wt.%) was added to 200 mL of boiling 1 mM $AgNO_3$ solution (0.01 wt.%). The mixture was refluxed for 1 h and then cooled to room temperature to obtain 55-nm bare Ag nanoparticles. A silica shell was added to the bare Ag nanoparticles using the method mentioned above[40].

Self-assembly of SHINs mono-layer film was prepared as follows. 10 μL 1 mM MG ethanol solution was dropped onto a quartz plate covered with a ~ 20 nm Au film. 10 mL SHINs solution was centrifuged at 5500 × *g* and washed with water three times. 3 mL cyclohexane and 5 mL 40 μM tetrabutyl-ammonium nitrate were then added into the concentrated solution. The solution was shaken and poured into a 10 mL beaker and stood to form two phases. A large and uniform monolayer of SHINs appeared at the interface between water and cyclohexane. The SHINs monolayer was then transferred onto the Au film.

The preparation of samples

Molecules (MG, PIC, pNTP) were adsorbed on Au/Ag films with self-assembled SHINs (Au or Ag cores, ~2 nm SiO_2 shell). The substrate was prepared by depositing a ~ 20 nm Au/Ag film on glass, followed by adsorption of 10^{-6} M MG, pNTP, or PIC in ethanol for 1 hour, and deposition of SHINs. Measurements were conducted in air at 25 °C.

FSRS Setup and Experimental protocol of SHINE-FSRS

We designed and built the experimental setup (Supplementary Fig. 13). Briefly, a femtosecond Ti: Sapphire laser system provides fundamental output at 800 nm (100 fs, 1 kHz) (Legend Elite-Duo-FS, Coherent). Part of the 800 nm output is used to pump a BBO to create the pump pulse at 400 nm (100 fs, 1 kHz). Another part of the 800 nm output is used to pump visible optical parametric amplifier (OPA) (Topas400-WL, Light conversion) after second harmonic bandwidth compressor (SHBC) to create the tunable picosecond Raman pump. The pulse duration is about 2.5 ps within the tuning range from 470 to 900 nm (with SHG 300–900 nm), and the line width is ~7 cm^{-1}. A super continuum white light generated by focusing a small portion of the fs 800 nm output into a 2 mm thick sapphire window is used as the Raman probe. The white light spectrum covers from 420 nm to 800 nm. In the SHINE-FSRS setup, the picosecond Raman pump (2.5 ps, 640 nm) and the femtosecond Raman probe (broadband, 420–800 nm) are temporally overlapped to optimize the stimulated Raman signal, with the delay between the 400 nm actinic pump and the Raman pump-probe pair varied to capture the ultrafast dynamics.

To obtain SHINE-FSRS signals of the MG molecule, we assembled the molecules on the Au film, then transferred the SHINs monolayer on them. Due to its strong enhancement ability, only trace amounts of molecules are needed to generate significant Raman signals. In order to figure out the best working condition of our home-built SHINE-FSRS[37], we use 4-nitrophenylthiophenol (pNPT) as a Raman probe to identify the enhancement of our equipment. pNPT molecules are chemically adsorbed on ~20 nm Au film plated on a 1 × 1 cm^2 Quartz sheet. A mono-layer Au SHINs is assembled onto the Quartz sheet. The SHINE-FSRS setup used a 400 nm actinic pump (100 fs, 70 nJ), a 640 nm Raman pump (2.5 ps, ~200 nJ), and a 420–800 nm Raman probe (300 fs, 20 nJ), with pulse energies optimized to avoid artifacts. Meanwhile, to prevent sample damage from excessively high pulse energy and to place more probe molecules within our detection field, we employ a defocused detection method, which moderately enhances the signal intensity. Notably, the molecules absorbed in the gap between the SHINs and the Au film experience a significant enhancement in Raman intensity, reaching up to ~10^7 times, owing to the strong near-field coupling between the localized surface plasmons (LSPs) of the SHINs and the surface plasmon polaritons (SPPs) of the gold film. The wavelength-dependent correlations between extinction spectra and SHINE-FSRS enhancement factors (EFs) were investigated. The ensemble-averaged enhancement factor is estimated to be in the range of 10^6–10^7 with the Raman pulse at 640 nm.

DFT calculations and optical simulations

The DFT calculations were performed using the Gaussian16 program suite (Supplementary table 1)[52]. The geometric structures optimization of malachite green molecules at different electronic states were carried out at the B3LYP/6-31 G* theoretical level. The Raman spectra of the molecule at each configuration were then calculated (Supplementary Fig. 10a).

The electromagnetic field distribution of Au/Ag SHINs dimer on the Au/Ag film surface under a 400 nm wavelength plane electromagnetic wave was calculated using commercially available Lumerical 3D-FDTD Solutions software. The diameter of the original Au/Ag NPs in the simulation was set as 55 nm. The thickness of the silica shell was set as 2 nm. The refined structure was 0.3 × 0.3 × 0.3 nm^3. The dielectric function of Au, Ag and silica was chosen from the material library of the software.

Data availability

The data generated or analysed during this study are included in this published article and its Supplementary information files. Source data are provided with this paper.

References

1. Dong, J.-C. et al. In situ Raman spectroscopic evidence for oxygen reduction reaction intermediates at platinum single-crystal surfaces. *Nat. Energy* **4**, 60–67 (2018).
2. Roithová, J. Characterization of reaction intermediates by ion spectroscopy. *Chem. Soc. Rev.* **41**, 547–559 (2012).
3. Carpenter, B. K. Energy disposition in reactive intermediates. *Chem. Rev.* **113**, 7265–7286 (2013).
4. Yan, M., Lo, J. C., Edwards, J. T. & Baran, P. S. Radicals: reactive intermediates with translational potential. *J. Am. Chem. Soc.* **138**, 12692–12714 (2016).
5. Huang, S.-C. et al. Probing nanoscale spatial distribution of plasmonically excited hot carriers. *Nat. Commun.* **11**, 4211 (2020).
6. Wang, H.-L., You, E.-M., Panneerselvam, R., Ding, S.-Y. & Tian, Z.-Q. Advances of surface-enhanced Raman and IR spectroscopies: from nano/microstructures to macro-optical design. *Light Sci. Appl.* **10**, 161 (2021).

7. Zhang, X. et al. Transient localized surface plasmon induced by femtosecond interband excitation in gold nanoparticles. *Sci. Rep.* **8**, 10499 (2018).
8. Manser, J. S. & Kamat, P. V. Band filling with free charge carriers in organometal halide perovskites. *Nat. Photonics* **8**, 737–743 (2014).
9. McCamant, D. W., Kukura, P., Yoon, S. & Mathies, R. A. Femtosecond broadband stimulated Raman spectroscopy: Apparatus and methods. *Rev. Sci. Instrum.* **75**, 4971–4980 (2004).
10. Kukura, P., McCamant, D. W. & Mathies, R. A. Femtosecond stimulated Raman spectroscopy. *Annu. Rev. Phys. Chem.* **58**, 461–488 (2007).
11. Dietze, D. R. & Mathies, R. A. Femtosecond stimulated Raman spectroscopy. *Chem. Phys. Chem.* **17**, 1224–1251 (2016).
12. Batignani, G., Ferrante, C., Fumero, G., Martinati, M. & Scopigno, T. Femtosecond stimulated Raman spectroscopy. *Nat. Rev. Methods Prim.* **4**, 34 (2024).
13. McCamant, D. W., Kukura, P. & Mathies, R. A. Femtosecond time-resolved stimulated Raman spectroscopy: application to the ultrafast internal conversion in β-carotene. *J. Phys. Chem. A* **107**, 8208–8214 (2003).
14. Zhao, B., Niu, K., Li, X. & Lee, S.-Y. Simple aspects of femtosecond stimulated Raman spectroscopy. *Sci. China Chem.* **54**, 1989–2008 (2011).
15. Frontiera, R. R., Fang, C., Dasgupta, J. & Mathies, R. A. Probing structural evolution along multidimensional reaction coordinates with femtosecond stimulated Raman spectroscopy. *Phys. Chem. Chem. Phys.* **14**, 405–414 (2012).
16. Kuramochi, H. & Tahara, T. Tracking ultrafast structural dynamics by time-domain Raman spectroscopy. *J. Am. Chem. Soc.* **143**, 9699–9717 (2021).
17. Fang, C., Frontiera, R. R., Tran, R. & Mathies, R. A. Mapping GFP structure evolution during proton transfer with femtosecond Raman spectroscopy. *Nature* **462**, 200–204 (2009).
18. Liu, W., Han, F., Smith, C. & Fang, C. Ultrafast Conformational Dynamics of Pyranine during Excited State Proton Transfer in Aqueous Solution Revealed by Femtosecond Stimulated Raman Spectroscopy. *J. Phys. Chem. B* **116**, 10535–10550 (2012).
19. Kuramochi, H. et al. Ultrafast Raman observation of the perpendicular intermediate phantom state of stilbene photoisomerization. *Nat. Chem.* **16**, 22–27 (2024).
20. Li, J. F. et al. Shell-isolated nanoparticle-enhanced Raman spectroscopy. *Nature* **464**, 392–395 (2010).
21. Zhang, H. et al. In situ dynamic tracking of heterogeneous nanocatalytic processes by shell-isolated nanoparticle-enhanced Raman spectroscopy. *Nat. Commun.* **8**, 15447 (2017).
22. Wang, Y.-H. et al. In situ Raman spectroscopy reveals the structure and dissociation of interfacial water. *Nature* **600**, 81–85 (2021).
23. Li, J. F. et al. Surface analysis using shell-isolated nanoparticle-enhanced Raman spectroscopy. *Nat. Protoc.* **8**, 52–65 (2013).
24. Wang, Y.-H. et al. In situ electrochemical Raman spectroscopy and ab initio molecular dynamics study of interfacial water on a single-crystal surface. *Nat. Protoc.* **18**, 883–901 (2023).
25. Li, J.-F., Anema, J. R., Wandlowski, T. & Tian, Z.-Q. Dielectric shell isolated and graphene shell isolated nanoparticle enhanced Raman spectroscopies and their applications. *Chem. Soc. Rev.* **44**, 8399–8409 (2015).
26. Küstner, B. et al. SERS labels for red laser excitation: silica-encapsulated SAMs on tunable gold/silver nanoshells. *Angew. Chem. Int. Ed.* **48**, 1950–1953 (2009).
27. Schlücker, S. Surface-enhanced raman spectroscopy: concepts and chemical applications. *Angew. Chem. Int. Ed.* **53**, 4756–4795 (2014).
28. Zhao, B.-J. et al. Infrared free induction decay (IR-FID) of non-interfacial origin observed in the interfacial sum-frequency generation vibrational spectroscopy (SFG-VS). *J. Phys. Chem. C.* **128**, 1443–1456 (2024).
29. Shen, S. et al. Plasmon-enhanced second-harmonic generation nanorulers with ultrahigh sensitivities. *Nano Lett.* **15**, 6716–6721 (2015).
30. Luo, Y., Martin-Jimenez, A., Gutzler, R., Garg, M. & Kern, K. Ultrashort pulse excited tip-enhanced Raman spectroscopy in molecules. *Nano Lett.* **22**, 5100–5106 (2022).
31. Mandal, A. & Ziegler, L. D. Vibrational line shape effects in plasmon-enhanced stimulated Raman spectroscopies. *J. Chem. Phys.* **155**, 194701 (2021).
32. McAnally, M. O., McMahon, J. M., Van Duyne, R. P. & Schatz, G. C. Coupled wave equations theory of surface-enhanced femtosecond stimulated Raman scattering. *J. Chem. Phys.* **145**, 094106 (2016).
33. Heiman, D., Hellwarth, R. W., Levenson, M. D. & Martin, G. Raman-induced Kerr effect. *Phys. Rev. Lett.* **36**, 189–192 (1976).
34. Balakrishnan, G., Soldatova, A. V., Reid, P. J. & Spiro, T. G. Ultrafast charge transfer in nickel phthalocyanine probed by femtosecond Raman-induced Kerr effect spectroscopy. *J. Am. Chem. Soc.* **136**, 8746–8754 (2014).
35. Shim, S. & Mathies, R. A. Femtosecond Raman-induced Kerr effect spectroscopy. *J. Raman Spectrosc.* **39**, 1526–1530 (2008).
36. Kumar, V. et al. Low-noise, vibrational phase-sensitive chemical imaging by balanced detection RIKE. *J. Raman Spectrosc.* **46**, 109–116 (2015).
37. Pyrcz, P. & Gawinkowski, S. Advancements in surface-enhanced femtosecond stimulated Raman spectroscopy: exploring factors influencing detectability and shapes of spectra. *Nanophotonics* **14**, 1–12 (2025).
38. Zhang, Y.-J. et al. Probing the location of 3D hot spots in gold nanoparticle films using surface-enhanced raman spectroscopy. *Anal. Chem.* **91**, 5316–5322 (2019).
39. Chen, H. et al. Excitonic-vibrational interaction at 2D material/organic molecule interfaces studied by time-resolved sum frequency generation. *Nanomaterials* **14**, 1892 (2024).
40. Amirsalari, A., Razi, S. & Gawinkowski, S. Multimodal microscope system for hyperspectral imaging of scattering directionality and Raman excitation spectroscopy. *J. Raman Spectrosc.* **54**, 976–987 (2023).
41. Li, C.-Y. et al. Observation of inhomogeneous plasmonic field distribution in a nanocavity. *Nat. Nanotechnol.* **15**, 922–926 (2020).
42. Frontiera, R. R., Henry, A.-I., Gruenke, N. L. & Van Duyne, R. P. Surface-enhanced femtosecond stimulated raman spectroscopy. *J. Phys. Chem. Lett.* **2**, 1199–1203 (2011).
43. Kumar, P., Kuramochi, H., Takeuchi, S. & Tahara, T. Time-domain observation of surface-enhanced coherent raman scattering with 10^5–10^6 enhancement. *J. Phys. Chem. Lett.* **11**, 6305–6311 (2020).
44. Cen, Q., He, Y., Xu, M., Wang, J. & Wang, Z. Wavelength dependent resonance Raman band intensity of broadband stimulated Raman spectroscopy of malachite green in ethanol. *J. Chem. Phys.* **142**, 114201 (2015).
45. Luo, Y. et al. Malachite green: a long-buried water-soluble AIEgen with near-infrared fluorescence for living cell nucleus staining. *Chem. Commun.* **60**, 1452–1455 (2024).
46. Li, J. et al. Plasmon-induced resonance energy transfer for solar energy conversion. *Nat. Photonics* **9**, 601–607 (2015).
47. Pelton, M. Modified spontaneous emission in nanophotonic structures. *Nat. Photonics* **9**, 427–435 (2015).
48. Ghenuche, P. et al. Matching nanoantenna field confinement to FRET distances enhances förster energy transfer rates. *Nano Lett.* **15**, 6193–6201 (2015).
49. Bharadwaj, P. & Novotny, L. Spectral dependence of single molecule fluorescence enhancement. *Opt. Express* **15**, 14266 (2007).
50. Akselrod, G. M. et al. Probing the mechanisms of large Purcell enhancement in plasmonic nanoantennas. *Nat. Photonics* **8**, 835–840 (2014).

51. Fita, P., Punzi, A. & Vauthey, E. Local viscosity of binary water+glycerol mixtures at liquid/liquid interfaces probed by time-resolved surface second harmonic generation. *J. Phys. Chem. C.* **113**, 20705–20712 (2009).
52. Frisch, M. J. et al. Gaussian 16 revision C.01. Gaussian, Inc., Wallingford CT (2016).

Acknowledgements

This work was supported by the National Key Research and Development Program of China (2023YFE0120300, H.Z.), NSFC (52171222, H.Z.; 22525042, J.F.L.; T2293692, J.F.L.; 22361132532, J.F.L.; 22021001, J.F.L.), Industry-University-Research Joint Innovation Project of Fujian Province, China (2024H6023, H.Z.), Scientific and Technological Project of Yunnan Precious Metals Laboratory (YPML-20240502063, J.F.L.), the State Key Laboratory of Fine Chemicals, Dalian University of Technology (KF 2401, J.F.L.), and the Liaoning Binhai Laboratory (Grant No. 2024-05, J.F.L.).

Author contributions

J. F. Li and H. Zhang supervised the project and conceived the idea. J. Liu, Y. Gu and Z. Wang analyzed the results and participated in writing the manuscript. H.G. Sun and Y. He performed the experiments and wrote the manuscript with input from all authors. G. Yin and L. Y. Hu synthesized the materials. X. Zhang, S. Zheng, Z. Shi, and R. Gao performed the theoretical calculation study. Y. Yang, H. Liu, B. Hu, and J. L. Yang performed TA experiment and analysis. Y. H. Wang discussed the experimental results. All authors discussed the results and assisted during manuscript preparation.

Competing interests

The authors declare no competing interests.

Additional information

Supplementary information The online version contains supplementary material available at https://doi.org/10.1038/s41467-025-66454-9.

Correspondence and requests for materials should be addressed to Hua Zhang, Jinxuan Liu, Yu Gu, Zhaohui Wang or Jian-Feng Li.

Peer review information *Nature Communications* thanks Sylwester Gawinkowski and the other, anonymous, reviewer(s) for their contribution to the peer review of this work. A peer review file is available.

[1]State Key Laboratory of Fine Chemicals, Dalian University of Technology, Dalian 116024, China; Leicester International Institute, Dalian University of Technology, Panjin, China. [2]College of Materials, College of Chemistry and Chemical Engineering, State Key Laboratory of Physical Chemistry of Solid Surfaces, College of Physical Science and Technology, Key Laboratory of High Performance Ceramics Fibers, Fujian Key Laboratory of Advanced Materials, Xiamen University, Xiamen, China. [3]College of Geography and Environmental Engineering, Gannan Normal University, Ganzhou, China. [4]School of Material and Environmental Engineering, Hangzhou Dianzi University, Hangzhou, China. [5]College of Physics, Guizhou University, Guiyang, China. [6]Key Laboratory of Green Chemical Media and Reactions, Ministry of Education, Collaborative Innovation Center of Henan, Province for Green Manufacturing of Fine Chemicals, School of Chemistry and Chemical Engineering, Henan Normal University, Xinxiang, China. [7]Innovation Laboratory for Sciences and Technologies of Energy Materials of Fujian Province (IKKEM), Xiamen, China. [8]Liaoning Binhai Laboratory, Liaoning, China. [9]College of Chemistry, Chemical Engineering and Environment, Minnan Normal University, Zhangzhou, China. [10]These authors contributed equally: Hong-Gang Sun, Yuhan He. ✉e-mail: zhanghua@xmu.edu.cn; jinxuan.liu@dlut.edu.cn; ygu@xmu.edu.cn; zhwang@xmu.edu.cn; li@xmu.edu.cn